Backscatter-NOMA: A Symbiotic System of Cellular and Internet-of-Things Networks

QIANQIAN ZHANG[1,2], **(Student Member, IEEE), LIN ZHANG**[1,2],
YING-CHANG LIANG[2], **(Fellow, IEEE), AND POOI-YUEN KAM**[2], **(Fellow, IEEE)**

[1]National Key Laboratory of Science and Technology on Communications, University of Electronic Science and Technology of China, Chengdu 611731, China
[2]Center for Intelligent Networking and Communications, University of Electronic Science and Technology of China, Chengdu 611731, China

Corresponding author: Ying-Chang Liang (liangyc@ieee.org)

ABSTRACT *Non-orthogonal multiple access* (NOMA) is envisioned as a key technology to enhance the spectrum efficiency for 5G cellular networks. Meanwhile, *ambient backscatter communication* is a promising solution to the *Internet of Things* (IoT), due to its high spectrum efficiency and power efficiency. In this paper, we are interested in a symbiotic system of cellular and IoT networks and propose a backscatter-NOMA system, which incorporates a downlink NOMA system with a *backscatter device* (BD). In the proposed system, the *base station* (BS) transmits information to two cellular users according to the NOMA protocol, while a BD transmits its information over the BS signals to one cellular user using the passive radio technology. In particular, if the BS only serves the cellular user that decodes BD information, the backscatter-NOMA system turns into a *symbiotic radio* (SR) system. We derive the expressions of the outage probabilities and the ergodic rates and analyze the corresponding diversity orders and slopes for both backscatter-NOMA and SR systems. Finally, we provide the numerical results to verify the theoretical analysis and demonstrate the interrelationship between the cellular networks and the IoT networks.

INDEX TERMS Non-orthogonal multiple access (NOMA), Internet-of-Things (IoT), ambient backscatter communication (AmBC), symbiotic radio (SR), outage probability, ergodic rate.

I. INTRODUCTION

Non-orthogonal multiple access (NOMA) is an effective solution to accommodate the data traffic in 5G networks due to its spectrum-efficiency [1]–[6] and has stimulated the upsurge of interest from both academia and industry [7]–[16]. Different from the conventional *orthogonal multiple access* (OMA) techniques which allow only one user to access the networks in each orthogonal resource block (e.g., a time slot, a frequency channel, a spreading code, or an orthogonal spatial degree of freedom), NOMA enables more than one user to access the networks in the same resource block and distinguishes them by exploiting the power domain. Thus, NOMA system is more spectrum-efficient than conventional OMA system especially when one of the NOMA users is far away from the *base station* (BS) [3].

The associate editor coordinating the review of this manuscript and approving it for publication was Zhiyong Chen.

So far, NOMA system has been actively studied in [7]–[16]. Al-Imari *et al.* [7] considered an uplink NOMA transmission scheme for higher system transmission rate and optimized the sum rate for all users by allocating subcarrier and power. The outage probability and achievable sum data rate were analyzed for uplink NOMA in [8]. With respect to the downlink NOMA scenarios, the outage probability and ergodic sum rate are derived in [9] with randomly deployed users. References [10]–[12] provided the performance analysis of NOMA systems with *multiple-input multiple-output* (MIMO) technique. Apart from the original NOMA works mentioned above, a new NOMA scheme called *cooperative relaying based NOMA* (CR-NOMA) was proposed in [13] and has received significant attention [14]–[16], where the cooperative relaying was introduced into the original NOMA to obtain a spatial diversity.

Meanwhile, *ambient backscatter communication* (AmBC) is emerging as a spectrum- and power-efficient technology for green *Internet-of-Things* (IoT) [17]–[19]. In AmBC, there

are three components: ambient *radio-frequency* (RF) source, *backscatter device* (BD), and reader. The BD transmits its information to the reader by reflecting the signals from the ambient RF source, which could be a legacy transmitter, through intentionally varying its load impedance without using dedicated RF components [17]. The AmBC takes place over the same spectrum as the RF source, and thus is a promising solution to future IoT.

AmBC technology has recently attracted much attention from both academia and industry [17], [20]–[33]. In [20], the authors characterize the optimal RF source transmitted power and the optimal BD reflection coefficient to maximize the ergodic rate of the BD. The capacity of AmBC over legacy *orthogonal frequency division multiplexing* (OFDM) signal is derived in [21]. The transceiver design for AmBC has been studied extensively in [27]–[30], where the proposed schemes achieve comparable performance to the optimal detector with perfect channel state information under the same conditions in terms of *bit error rate* (BER) performance. Guo *et al.* [31] exploit the NOMA scheme to support massive BD connections.

A novel technique, referred to as *symbiotic radio* (SR) technique, is proposed in [34] for passive IoT using AmBC technique. In SR, the BD and the primary transmission form a symbiotic system, in which the primary transmitter (RF source) supports not only the primary transmission but also the IoT transmission, while the primary receiver is required to decode the information from the primary transmitter as well as the BD. Compared with AmBC, in SR, not only the RF source and the spectrum but also the receiver are shared with the primary transmission, and thus SR system can achieve better performance since the two types of transmissions can be jointly designed.

A. MOTIVATION AND CONTRIBUTIONS

In this paper, we propose a symbiotic system of cellular and IoT networks, referred to as backscatter-NOMA, which incorporates cellular NOMA and AmBC. In this system, a BS transmits information to one far-away cellular user and one nearby cellular user simultaneously in the same resource block. Meanwhile, a BD transmits its information to the nearby cellular user by reflecting the signals from the received BS signal. The far-away user only needs to decode its own information, while the nearby user needs to decode the information from both the BS and the BD, and thus the AmBC part can be viewed as an uplink NOMA. Therefore, in the proposed backscatter-NOMA, there exist two types of NOMA systems: a downlink NOMA system for cellular networks, and an uplink NOMA system for IoT networks.

For the far-away user, it decodes its own information by treating other signals as interference. For the nearby user, it decodes the information of the far-away user first, then its own information, followed by the BD information. There are two reasons for designing the decoding order in this way. First, the signal from the BS enters the backscatter link in a multiplicative way, and thus the nearby user can

decode the information from the BD only if the signal from the BS is known. Second, due to the double fading effect, the backscatter link signal is weaker than the direct link signal from the BS, and thus it is easier for the nearby user to decode the direct link signal first. Based on the above observations, we see that the backscatter-NOMA system is different from conventional NOMA system and AmBC system, and thus the existing algorithms on both NOMA and AmBC systems cannot be directly applied to analyze the performance of the backscatter-NOMA system.

Interestingly, if the BS only serves the cellular user that decodes the BD information, the backscatter-NOMA system turns into the SR system, proposed in [34], while if the BD does not work, the backscatter-NOMA system turns into a conventional NOMA system.

For the proposed backscatter-NOMA system, to understand how the NOMA and the SR affect each other, in this paper, we derive the closed-form expressions of the outage probabilities and ergodic rates for all relevant transmissions in the backscatter-NOMA system and the SR system. In addition, we analyze the diversity order in terms of outage probability and the slope in terms of ergodic rate for these two systems. Numerical results will be presented to verify the accuracy of our theoretical analysis and demonstrate the inter-relationship between the cellular networks and IoT networks.

B. ORGANIZATION

The rest of the paper is organized as follows. In Section II, we establish the backscatter-NOMA system model and describe the SR system model. The theoretical expressions are derived for the outage probability and the diversity gain are analyzed in Section III. The analytical expressions in terms of the ergodic rate are derived in Section IV. Section V presents substantial numerical and simulation results for performance comparison and analytical validation. Finally, the paper is concluded in Section VI.

C. NOTATIONS

The main notations used in this paper is shown as follows. $\mathcal{CN}(\mu, \sigma^2)$ denotes the complex Gaussian distribution with mean μ and variance σ^2. $\mathbb{E}_x(\cdot)$ denotes the statistical expectation of x. $F_X(\cdot)$ and $f_X(\cdot)$ denote the *cumulative distribution function* (CDF) and the *probability dense function* (PDF) of a random variable X, respectively. Notation $\propto$ represents "be proportional to".

II. SYSTEM MODEL

In this section, we will provide a backscatter-NOMA model, which incorporates the IoT system with the conventional cellular system, and then an SR model and a conventional NOMA system, which are the special cases of the backscatter-NOMA system.

Fig. 1 illustrates the downlink backscatter-NOMA system, which includes four nodes, namely, the BS, the BD, the nearby cellular user (User 1), and the far-away cellular user (User 2). Here, the BS transmits the superposition
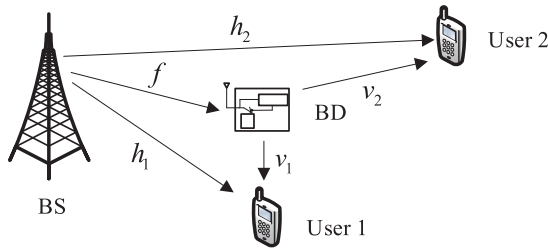
FIGURE 1. System Model.

message to User 1 and User 2 at the same resource block with different powers. The BD transmits its information to User 1 over the signal received from BS, and thus User 1 is also a IoT reader. In particular, User 1 decodes the information of User 2 first, then its own information, finally the BD information. This is achieved using *successive interference cancelation* (SIC) strategy. User 2, however, decodes its own information only.

As shown in Fig. 1, denote by h_1, h_2, and f the channel responses from the BS to User 1, User 2, and BD, respectively, and by v_1 and v_2 the channel responses from the BD to User 1 and User 2, respectively. Without loss of generality, let $h_1 \sim \mathcal{CN}(0, \lambda_1)$, $h_2 \sim \mathcal{CN}(0, \lambda_2)$, $f \sim \mathcal{CN}(0, \lambda_f)$, $v_1 \sim \mathcal{CN}(0, \lambda_{v,1})$, and $v_2 \sim \mathcal{CN}(0, \lambda_{v,2})$. In what follows, we provide the received signal and *signal-to-interference-plus-noise ratio* (SINR) models at User 1 and User 2.

A. RECEIVED SIGNALS AT USER 1
The superposition message at the BS can be written as

$$x(t) = \sqrt{\alpha p} x_1(t) + \sqrt{(1-\alpha)p} x_2(t), \qquad (1)$$

where $x_1(t)$ and $x_2(t)$ are the messages with unit power transmitted to User 1 and User 2, respectively, and p is the total transmit power of the BS with power allocation parameters α and $1 - \alpha$ to $x_1(t)$ and $x_2(t)$, respectively, with $0 \leq \alpha \leq 1$.

The BD backscatters the BS signal to User 1 with its own message $c(t)$, where $\mathbb{E}[|c(t)|^2] = 1$. Thus, User 1 receives two types of signals: direct link signal from the BS and the backscatter link signal from the BD. The received signals at User 1 can thus be written as

$$y_1(t) = h_1 x(t) + \beta f v_1 x(t) c(t) + n_1(t), \qquad (2)$$

where β is a complex reflection coefficient used to normalize $c(t)$ and $n_1(t)$ is the complex Gaussian noise at User 1 with $n_1(t) \sim \mathcal{CN}(0, \sigma^2)$. In the following, the SINR and *signal-to-noise ratio* (SNR) are given with the assumption of perfect *channel state information* (CSI).

User 1 first decodes $x_2(t)$, then $x_1(t)$, and finally $c(t)$ with SIC technique. When decoding $x_2(t)$, the SINR is

$$\gamma_{1,2} = \frac{p(1-\alpha)|h_1|^2}{\alpha p|h_1|^2 + p|\beta|^2|f|^2|v_1|^2 + \sigma^2}. \qquad (3)$$

Provided that $x_2(t)$ can be decoded successfully, it can be subtracted from $y_1(t)$, and then User 1 decodes its own message

$x_1(t)$, in which the SINR is given by

$$\gamma_{1,1} = \frac{\alpha p|h_1|^2}{p|\beta|^2|f|^2|v_1|^2 + \sigma^2}. \qquad (4)$$

Further, conditioned on perfectly decoding $x_1(t)$, the BD message $c(t)$ can then be decoded at User 1 based on SIC technique. Given $x(t)$, the SNR to decode $c(t)$ at User 1 can be written as

$$\gamma_{1,c}|x = \frac{|\beta|^2|f|^2|v_1|^2|x(t)|^2}{\sigma^2}. \qquad (5)$$

B. RECEIVED SIGNALS AT USER 2
The received signals at User 2 can be written as

$$y_2(t) = h_2 x(t) + \beta f v_2 x(t) c(t) + n_2(t), \qquad (6)$$

where $n_2(t)$ is the complex Gaussian noise at User 2 and follows $n_2(t) \sim \mathcal{CN}(0, \sigma^2)$. User 2 only decodes its own message $x_2(t)$ by treating other signal components as interference. When decoding $x_2(t)$, the SINR is

$$\gamma_{2,2} = \frac{p(1-\alpha)|h_2|^2}{\alpha p|h_2|^2 + p|\beta|^2|f|^2|v_2|^2 + \sigma^2}. \qquad (7)$$

As shown in Fig. 1, if the BS does not serve User 2, the backscatter-NOMA system turns into an SR system. In this case, α is equal to 1, i.e., $x(t) = \sqrt{p} x_1(t)$. The received signal at User 1 in the SR system is expressed as (2). In SR, User 1 first decodes $x_1(t)$ then $c(t)$ and the corresponding SINR and SNR are given by (4) and (5) with $\alpha = 1$, respectively. If the BD does not exist, the backscatter-NOMA system turns into a conventional downlink NOMA system.

In the following, we will analyze the performance for backscatter-NOMA system and SR system in terms of outage probability and ergodic rate. Since the performance of conventional NOMA system has been analyzed in [9], and thus we omit it in this paper.

III. OUTAGE PROBABILITY
The outage probability is an important metric for performance analysis when the target rates of users are determined by their required *quality of service* (QoS). In this section, we will study the outage probability performance for the backscatter-NOMA system and the SR system.

A. OUTAGE PROBABILITY FOR BACKSCATTER-NOMA SYSTEM
The outage probability of User 2 is easier to analyze since User 2 only needs to decode its own information. Thus, in the following, we first develop the outage probability of User 2, and then the outage probability of User 1 followed by the BD outage probability.

1) OUTAGE PROBABILITY OF USER 2
According to NOMA protocol, the outage events of User 2 occur when User 2 cannot decode message $x_2(t)$ successfully. Denote by $\gamma_{2,T} = 2^{R_2} - 1$ the target SINR to decode

$x_2(t)$, where R_2 is the target rate for User 2. The outage probability of User 2 is expressed as

$$P_{out,2} = 1 - \Pr\{\gamma_{2,2} \geq \gamma_{2,T}\}. \tag{8}$$

The following theorem provides the outage probability of User 2.

Theorem 1: The outage probability of User 2 is given by

$$P_{out,2} = \begin{cases} 1, & a < \alpha \leq 1; \\ 1 - B_1, & \text{otherwise,} \end{cases} \tag{9}$$

where $a = \frac{1}{1+\gamma_{2,T}}$, $B_1 = \frac{-\lambda_2 Q_1}{\lambda_{v,2}} \text{Ei}(-\frac{\lambda_2 Q_1}{\lambda_{v,2}}) e^{\frac{\lambda_2 Q_1}{\lambda_{v,2}} - \frac{Q_2}{\lambda_2}}$ *with* $Q_1 = \frac{1-\alpha-\alpha\gamma_{2,T}}{\lambda_f \gamma_{2,T}|\beta|^2}$, $Q_2 = \frac{\gamma_{2,T}\sigma^2}{p(1-\alpha-\alpha\gamma_{2,T})}$, *and* $\text{Ei}(x) = \int_{-\infty}^{x} \frac{e^{\rho}}{\rho} d\rho$ *is the exponential integral function.*

Proof: Based on (7), we have $\Pr\{\gamma_{2,2} \geq \gamma_{2,T}\} = \Pr\{p|h_2|^2(1-\alpha-\alpha\gamma_{2,T}) \geq \gamma_{2,T}(p|\beta|^2|f|^2|v_2|^2 + \sigma^2)\}$. It can be easily seen that $\Pr\{\gamma_{2,2} \geq \gamma_{2,T}\} = 0$, when $1-\alpha-\alpha\gamma_{2,T} < 0$, i.e., $a < \alpha \leq 1$. The PDFs of $|h_2|^2$ and $|v_2|^2$ are $f_{|h_2|^2}(y) = \frac{1}{\lambda_2} e^{\frac{-y}{\lambda_2}}$ and $f_{|v_2|^2}(z) = \frac{1}{\lambda_{v,2}} e^{\frac{-z}{\lambda_{v,2}}}$, respectively. When $0 \leq \alpha \leq a$, we have

$$\begin{aligned} &\Pr\{\gamma_{2,2} \geq \gamma_{2,T}\} \\ &= \Pr\left\{|h_2|^2 \geq \frac{(p|\beta|^2|f|^2|v_2|^2+\sigma^2)\gamma_{2,T}}{p(1-\alpha-\alpha\gamma_{2,T})}\right\} \\ &= \int_0^{+\infty} \int_{\frac{\gamma_{2,T}(p|\beta|^2 v + \sigma^2)}{p(1-\alpha-\alpha\gamma_{2,T})}}^{+\infty} f_{|h_2|^2}(y) f_{|f|^2|v_2|^2}(v) dy dv \\ &= \int_0^{+\infty} e^{-\frac{\gamma_{2,T}(p|\beta|^2 v + \sigma^2)}{\lambda_2 p(1-\alpha-\alpha\gamma_{2,T})}} f_{|f|^2|v_2|^2}(v) dv \\ &\overset{(a)}{=} \frac{2}{\lambda_f \lambda_{v,2}} e^{-\frac{Q_2}{\lambda_2}} \int_0^{+\infty} e^{-\frac{\gamma_{2,T}|\beta|^2 v}{\lambda_2(1-\alpha-\alpha\gamma_{2,T})}} K_0\left(2\sqrt{\frac{v}{\lambda_f \lambda_{v,2}}}\right) dv \\ &\overset{(b)}{=} -\frac{\lambda_2 Q_1}{\lambda_{v,2}} \text{Ei}(-\frac{\lambda_2 Q_1}{\lambda_{v,2}}) e^{\frac{\lambda_2 Q_1}{\lambda_{v,2}} - \frac{Q_2}{\lambda_2}}, \end{aligned} \tag{10}$$

where (*a*) follows from Appendix A, $K_0(x)$ is the modified Bessel function of the second kind, and (*b*) is from Appendix B. Thus, Theorem 1 is proved. ∎

From Theorem 1, we find that $P_{out,2}$ is a segmented function related to the power allocation parameter α. When $a < \alpha \leq 1$, the outage probability is equal to 1. The main reason is that the received SINR at User 2 is less than the target SINR of User 2 due to the large power allocation parameter α. In practice, the distance between BD and User 2 is large, and thus the interference from the backscatter link is negligible, based on which, we have

$$\lim_{\lambda_{v,2}\to 0} P_{out,2} \overset{(a)}{=} \begin{cases} 1, & a < \alpha \leq 1; \\ 1 - e^{-\frac{\gamma_{2,T}\sigma^2}{\lambda_2 p(1-\alpha-\alpha\gamma_{2,T})}}, & \text{otherwise,} \end{cases} \tag{11}$$

where (a) follows from Appendix C. Eq. (11) indicates that when the distance between BD and User 2 is large, the outage probability of User 2 is the same as that in the traditional NOMA system, just related with the power allocation parameter α, the target SINR of User 2 $\gamma_{2,T}$, and the average channel strength from BS to User 2 λ_2. In this case, if $\alpha < a$ and

$p \to \infty$, we have $P_{out,2} = 0$, which means that when the power allocation parameter α satisfies $\alpha < a$, the outage probability of User 2 goes to zero with high transmit power p. In addition, from (11), it is seen that, the smaller the power allocation parameter α, the lower the outage probability of User 2 $P_{out,2}$, when $\lambda_{v,2} \to 0$, i.e., the distance between BD and User 2 is large.

2) OUTAGE PROBABILITY OF USER 1

With the backscatter-NOMA protocol, if User 1 fails to decode $x_1(t)$, we define this event as an outage event. To successfully decode $x_1(t)$, two conditions need to be met: 1) User 1 can decode $x_2(t)$ successfully, namely $\gamma_{1,2} \geq \gamma_{2,T}$; 2) User 1 can decode its own information $x_1(t)$ successfully, namely $\gamma_{1,1} \geq \gamma_{1,T}$. Denote by $\gamma_{1,T}$ the target SINR to decode $x_1(t)$, where $\gamma_{1,T} = 2^{R_1} - 1$ with R_1 the target rate for User 1. Then, the outage probability can be written as

$$P_{out,1} = 1 - \Pr\{\gamma_{1,2} \geq \gamma_{2,T}, \gamma_{1,1} \geq \gamma_{1,T}\}. \tag{12}$$

According to the following theorem, the outage probability $P_{out,1}$ can be obtained.

Theorem 2: The closed-form expression for the outage probability when decoding $x_1(t)$ at User 1 is given by

$$P_{out,1} = \begin{cases} 1, & a < \alpha \leq 1, \alpha = 0; \\ 1 - B_2, & b < \alpha \leq a; \\ 1 - B_3, & 0 < \alpha \leq b, \end{cases} \tag{13}$$

where $b = \frac{\gamma_{1,T}}{\gamma_{2,T}+\gamma_{1,T}+\gamma_{2,T}\gamma_{1,T}}$, $B_2 = \frac{-\lambda_1 Q_1}{\lambda_{v,1}} \text{Ei}(-\frac{\lambda_1 Q_1}{\lambda_{v,1}}) e^{\frac{\lambda_1 Q_1}{\lambda_{v,1}} - \frac{Q_2}{\lambda_1}}$, *and* $B_3 = -\alpha Q_3 \text{Ei}(-\alpha Q_3) e^{\alpha Q_3 - \frac{\gamma_{1,T}\sigma^2}{p\lambda_1\alpha}}$ *with* $Q_3 = \frac{\lambda_1}{\lambda_f \lambda_{v,1} \gamma_{1,T}|\beta|^2}$.

Proof: The details are given in Appendix D. ∎

From Theorem 2, it is easy to see that when $a < \alpha \leq 1$, the outage event always occurs for User 1, which is similar to case for $P_{out,2}$. The reason is that User 1 needs to decode $x_2(t)$ before $x_1(t)$. Hence, if User 1 fails to decode $x_2(t)$ due to the high α, the outage event happens. Furthermore, when $\alpha = 0$, all transmit power p is allocated to the message of User 2, thereby outage event occurs for User 1. Next, we consider the effect of the BD on $P_{out,1}$. If $|\beta|^2$ goes to zero, i.e., the received energy from the backscatter link is low, according to Appendix C, we have the following insights: when $a < \alpha \leq 1$, or $\alpha = 0$, the outage probability of User 1 is 1; when $b < \alpha \leq a$, the outage probability of User 1 is $1 - e^{-\frac{\gamma_{2,T}\sigma^2}{\lambda_1 p(1-\alpha-\alpha\gamma_{2,T})}}$; finally, when $0 < \alpha \leq b$, the outage probability of User 1 is $1 - e^{-\frac{\gamma_{1,T}\sigma^2}{p\lambda_1\alpha}}$. The insights for $P_{out,1}$ with $|\beta|^2 \to 0$ are similar to that in the conventional NOMA system with two users, i.e., $\lim_{|\beta|^2 \to 0, p \to \infty} P_{out,1} = 0$, when $\alpha \leq a, \alpha \neq 0$. Furthermore, there is a trade-off phenomenon due to the power allocation parameter α. When α increases, it is more difficult to decode $x_2(t)$, which may result in the outage event for User 1, due to SIC. When α decreases, it is more difficult to decode $x_1(t)$, which also may result in the outage event for User 1.

3) OUTAGE PROBABILITY OF BD

Based on backscatter-NOMA protocol, if User 1 fails to decode $c(t)$, we consider this event as the outage event of BD. From (5), the SNR expression contains the BS transmitted message $x(t)$, which changes fast. For this case, according to [35], the BD rate can be written as

$$
\begin{aligned}
R_c &= \mathbb{E}_x \left[\log_2 \left(1 + \frac{|\beta|^2 |f|^2 |v_1|^2 |x(t)|^2}{\sigma^2} \right) \right] \\
&\stackrel{(a)}{=} \frac{-1}{\ln 2} e^{\frac{\sigma^2}{p|\beta|^2 |f|^2 |v_1|^2}} \mathrm{Ei} \left(-\frac{\sigma^2}{p|\beta|^2 |f|^2 |v_1|^2} \right),
\end{aligned} \tag{14}
$$

where (a) follows from [36]. We define the ergodic SNR of BD as $\bar{\gamma}_{1,c} \triangleq \frac{p|\beta|^2 |f|^2 |v_1|^2}{\sigma^2}$. Since R_c is a monotonically increasing function of $\bar{\gamma}_{1,c}$, we use $\gamma_{c,T}$ as the target ergodic SNR corresponding to target rate $R_{c,T}$ for decoding BD signals. The BD message can be successfully decoded conditioned on perfectly decoded $x_2(t)$ and $x_1(t)$. Thus, the outage probability of BD is given by

$$
P_{out,c} = 1 - \Pr\{\gamma_{1,2} \geq \gamma_{2,T}, \gamma_{1,1} \geq \gamma_{1,T}, \bar{\gamma}_{1,c} \geq \gamma_{c,T}\}. \tag{15}
$$

The exact expression of the BD outage probability P_{outc} is provided in the following theorem.

Theorem 3: The outage probability of BD is given by

$$
P_{out,c} = \begin{cases} 1, & a < \alpha \leq 1, \alpha = 0; \\ 1 - B_2 + B_4, & b < \alpha \leq a; \\ 1 - B_3 + B_5, & 0 < \alpha \leq b, \end{cases} \tag{16}
$$

where $B_4 \approx \frac{\pi \gamma_{c,T} \sigma^2}{K|\beta|^2 p \lambda_f \lambda_{v,1}} e^{-\frac{Q_2}{\lambda_1}} \sum_{k=1}^{K} \sqrt{1 - \phi_k^2} K_0 (Q_4)$
$e^{-\frac{\gamma_{c,T}(\phi_k+1)Q_2}{2\lambda_1}}$, $B_5 \approx \frac{\pi \gamma_{c,T} \sigma^2}{K|\beta|^2 p \lambda_f \lambda_{v,1}} e^{-\frac{\gamma_{1,T} \sigma^2}{\lambda_1 p \alpha}}$
$\sum_{k=1}^{K} \sqrt{1 - \phi_k^2} e^{-\frac{\gamma_{1,T} \gamma_{c,T} \sigma^2 (\phi_k+1)}{2\lambda_1 p \alpha}}$ $K_0 (Q_4)$, *with* $Q_4 = 2\sqrt{\frac{\gamma_{c,T} \sigma^2 (\phi_k+1)}{2|\beta|^2 p \lambda_f \lambda_{v,1}}}$, $\phi_k = \cos[(2k-1)\pi/(2K)]$, *and* K *is an accuracy-complexity tradeoff parameter.*

Proof: The details are given in Appendix E. ∎

Theorem 3 indicates that the outage probability of BD is related to the outage probability of User 1. When $\alpha \leq a, \alpha \neq 0$, we have $P_{out,c} > P_{out,1}$. The reason is that User 1 decodes $x_1(t)$ before $c(t)$. If User 1 fails to decode $x_1(t)$, the outage event for BD happens. When the backscatter link SNR is low, according to Theorem 2, we know $P_{out,1} \to 0$, while according to Theorem 3, the outage probability of BD $P_{out,c} \to 1$. This phenomenon indicates that when the received energy of the backscatter link is low, it is easier for User 1 to decode its own message successfully, but it is more difficult for User 1 to decode the message from BD. Hence, there is a trade-off between the outage probability of User 1 and that of BD about the reflection coefficient β.

B. OUTAGE PROBABILITY FOR THE SR SYSTEM

In this subsection, we first provide the outage probability of User 1 and then the outage probability of BD.

1) OUTAGE PROBABILITY OF USER 1

For SR, if User 1 can not decode $x_1(t)$ successfully, we define this event as the outage event. The outage probability of User 1 in SR is given by $P_{out,1}^{SR} = 1 - \{\gamma_{1,1} \geq \gamma_{1,T}\}$. According to Appendix D, the outage of User 1 in SR is

$$
P_{out,1}^{SR} = 1 + Q_3 \mathrm{Ei}(-Q_3) e^{Q_3 - \frac{\gamma_{1,T} \sigma^2}{p \lambda_1}}, \tag{17}
$$

In contrast to $P_{out,1}$, $P_{out,1}^{SR}$ is not a segmented function since the BS does not need to allocate power in SR. Similar to III-A.2, when $p \to \infty$ and $|\beta|^2 \to 0$, we have $P_{out,1}^{SR} \to 0$.

2) OUTAGE PROBABILITY OF BD

If User 1 fails to decode $x_1(t)$ or $c(t)$, the outage event for BD occurs, and thus the outage probability of BD can be expressed as $P_{out,c}^{SR} = 1 - \Pr\{\gamma_{1,1} \geq \gamma_{1,T}, \bar{\gamma}_{1,c} \geq \gamma_{c,T}\}$. Similar to Appendix E, $P_{out,c}^{SR}$ is given by

$$
\begin{aligned}
P_{out,c}^{SR} &= 1 + Q_3 \mathrm{Ei}(-Q_3) e^{Q_3 - \frac{\gamma_{1,T} \sigma^2}{p \lambda_1}} + \frac{\pi \gamma_{c,T} \sigma^2}{pK|\beta|^2 \lambda_f \lambda_{v,1}} \\
&\quad \times e^{-\frac{\gamma_{1,T} \sigma^2}{\lambda_1 p \alpha}} \sum_{k=1}^{K} \sqrt{1 - \phi_k^2} e^{-\frac{\gamma_{1,T} \gamma_{c,T} \sigma^2 (\phi_k+1)}{2\lambda_1 p \alpha}} K_0(Q_4),
\end{aligned} \tag{18}
$$

As in Section III-A.3, there is a trade-off using the reflection coefficient β in $P_{out,c}^{SR}$.

C. DIVERSITY ORDER

To get more insights, we provide the asymptotic diversity order analysis in terms of outage probability in high SNR region. The definition of diversity order with outage probability is given by

$$
d = -\lim_{p \to \infty} \frac{\log_{10} P_{out}(p)}{\log_{10} p}. \tag{19}
$$

1) OUTAGE PROBABILITY OF USER 2 IN BACKSCATTER-NOMA

Based on the result in (9), when the transmit power p goes to infinity, we have $P_{out,2} = C$, where C represents a constant. Hence, according to the definition in (19), the diversity order with outage probability for User 2 is $d_2 = 0$. The main reason is that when the transmit power increases, the interference from the BD increases. However, since the distance between User 2 and BD is usually large, the interference from backscatter link is negligible for User 2. In this case, based on (11), when $\alpha < a$ and p is large, the asymptotic outage probability of User 2, with $e^{-x} \approx 1 - x$, is given by

$$
\lim_{\lambda_{v,2} \to 0} P_{out,2} \propto \frac{1}{p}.
$$

Therefore, the diversity order in terms of outage probability for User 2 is $\lim_{\lambda_{v,2} \to \infty} d_2 = 1$.

2) OUTAGE PROBABILITY OF USER 1 IN BACKSCATTER-NOMA

From (13), it is seen that when the transmit power from BS goes to infinity, the outage probability of User 1 becomes a constant. The diversity order with outage probability for User 1 thus is $d_1 = 0$.

3) OUTAGE PROBABILITY OF BD IN BACKSCATTER-NOMA

It is difficult to analyze the diversity order in terms of outage probability for BD according to (16) directly. However, we have stated that $P_{out,c} \geqslant P_{out,1}$. Since $d_1 = 0$, we have that the diversity order in terms of outage probability for BD is $d_c = 0$.

4) OUTAGE PROBABILITY OF USER 1 IN SR

From Section III-B.1, when $p \to \infty$, $P_{out,1}^{SR}$ becomes a constant. Thus, the diversity order in terms of outage probability for User 1 in SR is $d_1^{SR} = 0$.

5) OUTAGE PROBABILITY OF BD IN SR

Similar to Section III-C.3, the diversity order in terms of outage probability for BD in SR is $d_c^{SR} = 0$.

IV. ERGODIC RATE

The ergodic rate is an important metric for performance analysis when the rates of users are determined by their channel conditions. Hence, in this section, we analyze the ergodic rates for all relevant transmissions in the backscatter-NOMA system and the SR system.

A. ERGODIC RATE FOR BACKSCATTER-NOMA SYSTEM

1) ERGODIC RATE FROM BS TO USER 1

In this subsection, we provide the ergodic rate from BS to User 1. On the condition that User 1 detects $x_2(t)$ perfectly, the ergodic rate from BS to User 1 is given by

$$R_{U,1}^{(e)} = \mathbb{E}\left[\log_2(1 + \frac{\alpha p |h_1|^2}{p|\beta|^2|f|^2|v_1|^2 + \sigma^2})\right] \quad (20)$$

By letting $\theta = \frac{\alpha p |h_1|^2}{|\beta|^2 p |f|^2 |v_1|^2 + \sigma^2}$, (20) can be rewritten as

$$R_{U,1}^{(e)} = \mathbb{E}[\log_2(1+\theta)] = \int_0^{+\infty} \log(1+\theta) f_\theta(\theta) d\theta$$
$$= \frac{1}{\ln 2} \int_0^{+\infty} \frac{1 - F_\Theta(\theta)}{1 + \theta} d\theta, \quad (21)$$

where $f_\theta(\theta)$ is the PDF of the random variable θ and $F_\theta(\theta)$ is the CDF of the random variable θ.

According to the definition of CDF, $F_\theta(\theta)$ in (21) is given by

$$F_\Theta(\theta) = \Pr\left(\frac{\alpha p |h_1|^2}{p|\beta|^2|f|^2|v_1|^2 + \sigma^2} < \theta\right)$$
$$= \Pr\left(|h_1|^2 < \frac{p|\beta|^2|f|^2|v_1|^2\theta + \sigma^2\theta}{\alpha p}\right) \quad (22)$$

The PDFs of $|h_1|^2$, $|f|^2$, and $|v_1|^2$ are $f_{|h_1|^2}(x) = \frac{1}{\lambda_1}e^{\frac{-x}{\lambda_1}}$, $f_{|f|^2}(u) = \frac{1}{\lambda_f}e^{\frac{-u}{\lambda_f}}$, and $f_{|v_1|^2}(w) = \frac{1}{\lambda_{v,1}}e^{\frac{-w}{\lambda_{v,1}}}$, respectively. Then $F_\theta(\theta)$ in (22) can be calculated as

$$F_\Theta(\theta) = \Pr\left(|h_1|^2 < \frac{p|\beta|^2|f|^2|v_1|^2\theta + \sigma^2\theta}{\alpha p}\right)$$
$$= \int_0^{+\infty} \left(1 - e^{\frac{p|\beta|^2v\theta + \sigma^2\theta}{\alpha p \lambda_1}}\right) \frac{2}{\lambda_f \lambda_{v,1}} K_0\left(2\sqrt{\frac{v}{\lambda_f \lambda_{v,1}}}\right) dv$$
$$= \int_0^{+\infty} \frac{2}{\lambda_f \lambda_{v,1}} K_0\left(2\sqrt{\frac{v}{\lambda_f \lambda_{v,1}}}\right) dv$$
$$- \int_0^{+\infty} \frac{2}{\lambda_f \lambda_{v,1}} e^{\frac{p|\beta|^2v\theta + \sigma^2\theta}{\alpha p \lambda_1}} K_0\left(2\sqrt{\frac{v}{\lambda_f \lambda_{v,1}}}\right) dv$$
$$\overset{(a)}{=} 1 - \frac{2}{\lambda_f \lambda_{v,1}} \int_0^{+\infty} e^{\frac{p|\beta|^2v\theta + \sigma^2\theta}{\alpha p \lambda_1}} K_0\left(2\sqrt{\frac{v}{\lambda_f \lambda_{v,1}}}\right) dv$$
$$\overset{(b)}{=} 1 + \frac{Q_5}{\theta} \text{Ei}\left(\frac{-Q_5}{\theta}\right) e^{\frac{Q_5}{\theta} - \frac{\sigma^2\theta}{\alpha p \lambda_1}}, \quad (23)$$

where (a) is obtained according to Appendix F, and (b) follows from Appendix B, and $Q_5 = \frac{\alpha \lambda_1}{\lambda_f \lambda_{v,1} |\beta|^2}$.

Substituting (23) into (21), $R_{U,1}^{(e)}$ can be calculated as

$$R_{U,1}^{(e)} = \frac{1}{\ln 2} \int_0^{+\infty} \frac{-Q_5}{\theta(1+\theta)} \text{Ei}\left(\frac{-Q_5}{\theta}\right) e^{\frac{Q_5}{\theta} - \frac{\sigma^2\theta}{\alpha p \lambda_1}} d\theta. \quad (24)$$

From (24), we find it is difficult to obtain an accurate closed-form expression for $R_{U,1}^{(e)}$, and thus we provide the following theorem for numerical analysis.

Theorem 4: The function $f(\theta) = \frac{-\varepsilon}{\theta(1+\theta)}\text{Ei}\left(-\frac{\varepsilon}{\theta}\right) e^{\frac{\varepsilon}{\theta} - \varsigma\theta}$ decreases with θ and $\lim_{\theta \to \infty} f(\theta) = 0$, where $\varepsilon > 0$, $\varsigma > 0$, and $\theta > 0$.

Proof: The first derivative of $f(\theta)$ is given by

$$f'(\theta) = \frac{\varepsilon e^{-\varsigma\theta}}{\theta^3(\theta+1)^2}$$
$$\times \left[\text{Ei}(-\varepsilon/\theta)(\varsigma\theta^3 + \varsigma\theta^2 + 2\theta^2 + \varepsilon\theta + \theta + \varepsilon)e^{\frac{\varepsilon}{\theta}} + \theta(\theta+1)\right].$$

Since $\text{Ei}\left(-\frac{\varepsilon}{\theta}\right) < 0$ we have $f'(\theta) < 0$. Thus $f(\theta)$ decreases with θ. In addition, when $\theta \to \infty$, it is easy to find $e^{\frac{\varepsilon}{\theta}} = 1$. For other parts of $f(\theta)$, we have

$$\lim_{\theta \to \infty} \frac{-\varepsilon}{\theta(1+\theta)} \text{Ei}\left(-\frac{\varepsilon}{\theta}\right) e^{-\varsigma\theta}$$
$$= \lim_{\theta \to \infty} \frac{-\varepsilon}{\theta(1+\theta)e^{\varsigma\theta}} \text{Ei}\left(-\frac{\varepsilon}{\theta}\right)$$
$$= \lim_{\theta \to \infty} \frac{\varepsilon e^{-\frac{\varepsilon}{\theta}}}{\theta e^{\varsigma\theta}(1 + 2\theta + \varsigma\theta + \varsigma\theta^2)} = 0.$$

Therefore, $\lim_{\theta \to \infty} f(\theta) = 0$. ∎

From Theorem 4, when M is a large number, we have $\int_M^{+\infty} \frac{-Q_5}{\theta(1+\theta)} \text{Ei}\left(\frac{-Q_5}{\theta}\right) e^{\frac{Q_5}{\theta} - \frac{\sigma^2\theta}{\alpha p \lambda_1}} d\theta \to 0$, and thus we obtain

$$R_{U,1}^{(e)} \approx \frac{1}{\ln 2} \int_0^M \frac{-Q_5}{\theta(1+\theta)} \text{Ei}\left(\frac{-Q_5}{\theta}\right) e^{\frac{Q_5}{\theta} - \frac{\sigma^2\theta}{\alpha p \lambda_1}} d\theta. \quad (25)$$

Applying Gaussian-Chebyshev quadrature, we have

$$R_{U,1}^{(e)} \approx \frac{-2\pi M Q_5}{K \ln 2} \sum_{k=1}^{K} \frac{\sqrt{1-\phi_k^2}}{(M\phi_k + M)(M\phi_k + M + 2)}$$
$$\times \text{Ei}\left(\frac{-2Q_5}{(M\phi_k + M)}\right) e^{\frac{2Q_5}{(M\phi_k + M)} - \frac{\sigma^2(M\phi_k + M)}{2\alpha p \lambda_1}}. \quad (26)$$

2) ERGODIC RATE FROM BS TO USER 2

In this part, we provide the ergodic rate from BS to User 2. If we let $\psi = \frac{p(1-\alpha)|h_2|^2}{\alpha p|h_2|^2 + p|\beta|^2|f|^2|v_2|^2 + \sigma^2}$, we obtain

$$R_{U,2}^{(e)} = \mathbb{E}\left[\log_2(1 + \frac{p(1-\alpha)|h_2|^2}{\alpha p|h_2|^2 + p|\beta|^2|f|^2|v_2|^2 + \sigma^2})\right]$$
$$= \mathbb{E}[\log_2(1+\psi)] = \frac{1}{\ln 2} \int_0^{+\infty} \frac{1 - F_\Psi(\psi)}{1 + \psi} d\psi. \quad (27)$$

Since $F_\Psi(\psi) = \Pr\left(\frac{p(1-\alpha)|h_2|^2}{\alpha p|h_2|^2 + p|\beta|^2|f|^2|v_2|^2 + \sigma^2} < \psi\right) = \Pr\left(p(1 - \alpha - \alpha\psi)|h_2|^2 < \psi(p|\beta|^2|f|^2|v_2|^2 + \sigma^2)\right)$, it is straightforward that when $1 - \alpha - \alpha\psi < 0$, i.e., $\psi > 1/\alpha - 1$, we obtain $F_\Psi(\psi) = 0$. When $1 - \alpha - \alpha\psi > 0$, we have

$$F_\Psi(\psi) = \Pr\left(|h_2|^2 < \frac{\psi(p|\beta|^2|f|^2|v_2|^2 + \sigma^2)}{p(1 - \alpha - \alpha\psi)}\right)$$
$$= 1 + \frac{Q_6}{\psi} \text{Ei}(\frac{-Q_6}{\psi}) e^{\frac{Q_6}{\psi} - \frac{\psi\sigma^2}{\lambda_2 p(1-\alpha-\alpha\psi)}}, \quad (28)$$

where $Q_6 = \frac{\lambda_2(1-\alpha-\alpha\psi)}{\lambda_f \lambda_{v,2}|\beta|^2}$. Substituting (28) into (27), we have

$$R_{U,2}^{(e)} = \frac{1}{\ln 2} \int_0^{\frac{1}{\alpha}-1} \frac{-Q_6}{\psi(1+\psi)} \text{Ei}\left(\frac{-Q_6}{\psi}\right) e^{\frac{Q_6}{\psi} - \frac{\sigma^2\psi}{p\lambda_2(1-\alpha-\alpha\psi)}} d\psi.$$

Then, applying Gaussian-Chebyshev quadrature, we have

$$R_{U,2}^{(e)} \approx \frac{-\pi Q_7}{K \ln 2} \sum_{k=1}^{K} \text{Ei}\left(\frac{-\alpha(1-\phi_k)Q_7}{(\phi_k+1)}\right) e^{\frac{\alpha(1-\phi_k)Q_7}{(\phi_k+1)} - \frac{\sigma^2(\phi_k+1)}{\alpha p \lambda_2(1-\phi_k)}}$$
$$\times \frac{\alpha(1-\alpha)(1-\phi_k)\sqrt{1-\phi_k^2}}{(\phi_k+1)[2\alpha + (1-\alpha)(\phi_k+1)]}, \quad (29)$$

where $Q_7 = \frac{\lambda_2}{\lambda_f \lambda_{v,2}|\beta|^2}$.

3) ERGODIC RATE FROM BD TO USER 1

The rate from BD to User 1 can be written as

$$R_c^{(e)} = \mathbb{E}_{f,v_1,x}\left[\log_2\left(1 + \frac{|\beta|^2|f|^2|v_1|^2|x(t)|^2}{\sigma^2}\right)\right] \quad (30)$$

Using the definition of expectation, we have (31) on the bottom of the next page. When w is large, it is easy to show that $\frac{-1}{\lambda_f \lambda_{v,1} \ln 2} e^{-\frac{w}{\lambda_{v,1}} + \frac{\sigma^2}{p|\beta|^2 uw}} \text{Ei}\left(-\frac{\sigma^2}{p|\beta|^2 uw}\right)$ decreases with w. Thus using the approximation in (25), the term B_6 in (31) can be approximated as

$$B_6 \approx \int_0^M \frac{-1}{\lambda_f \lambda_{v,1} \ln 2} e^{-\frac{w}{\lambda_{v,1}} + \frac{\sigma^2}{p|\beta|^2 uw}} \text{Ei}\left(-\frac{\sigma^2}{p|\beta|^2 uw}\right) dw, \quad (32)$$

where M is a large value. Applying Gaussian-Chebyshev quadrature, we have

$$B_6 \approx \frac{-M\pi}{2K\lambda_f \lambda_{v,1} \ln 2} \sum_{k=1}^{K} \sqrt{1 - \phi_k^2} e^{\frac{2\sigma^2}{p|\beta|^2 u(M\phi_k + M)} - \frac{M\phi_k + M}{2\lambda_{v,1}}}$$
$$\times \text{Ei}\left(-\frac{2\sigma^2}{p|\beta|^2 u(M\phi_k + M)}\right). \quad (33)$$

Substituting (33) into (31), we have

$$R_c^{(e)} \approx \int_0^{+\infty} \frac{-M\pi}{2K\lambda_f \lambda_{v,1} \ln 2} \sum_{k=1}^{K} e^{\frac{2\sigma^2}{p|\beta|^2 u(M\phi_k + M)} - \frac{M\phi_k + M}{2\lambda_{v,1}} - \frac{u}{\lambda_f}}$$
$$\times \sqrt{1 - \phi_k^2} \text{Ei}\left(-\frac{2\sigma^2}{p|\beta|^2 u(M\phi_k + M)}\right) du. \quad (34)$$

It is difficult to obtain a closed-form expression for (34). Thus we again use the approximation in (25) and obtain

$$R_c^{(e)} \approx \int_0^M \frac{-M\pi}{2K\lambda_f \lambda_{v,1} \ln 2} \sum_{k=1}^{K} e^{\frac{2\sigma^2}{p|\beta|^2 u(M\phi_k + M)} - \frac{M\phi_k + M}{2\lambda_{v,1}} - \frac{u}{\lambda_f}}$$
$$\times \sqrt{1 - \phi_k^2} \text{Ei}\left(-\frac{2\sigma^2}{p|\beta|^2 u(M\phi_k + M)}\right) du, \quad (35)$$

Applying Gaussian-Chebyshev quadrature, we have

$$R_c^{(e)} \approx \frac{-M^2\pi^2}{4KN\lambda_f \lambda_{v,1} \ln 2} \sum_{k=1}^{K} \sqrt{1 - \phi_k^2} \sum_{n=1}^{N} \sqrt{1 - \varphi_n^2}$$
$$\times \text{Ei}\left(-\frac{4\sigma^2}{p|\beta|^2(M\phi_k + M)(M\varphi_n + M)}\right)$$
$$\times e^{\frac{4\sigma^2}{p|\beta|^2(M\phi_k + M)(M\varphi_n + M)} - \frac{M\phi_k + M}{2\lambda_{v,1}} - \frac{M\varphi_n + M}{2\lambda_f}}, \quad (36)$$

where $\varphi_n = \cos[(2n - 1)\pi/(2N)]$ and N is an accuracy-complexity tradeoff parameter.

B. ERGODIC RATE FOR SR SYSTEM

1) ERGODIC RATE FROM BS TO USER 1

In SR, the ergodic rate from BS to User 1 can be written as

$$R_{U,1}^{SR} = \mathbb{E}\left[\log_2(1 + \frac{p|h_1|^2}{p|\beta|^2|f|^2|v_1|^2 + \sigma^2})\right], \quad (37)$$

which is equal to (20) with $\alpha = 1$. Thus the ergodic rate from BS to User 1 in SR is equal to (26) with $\alpha = 1$.

2) ERGODIC RATE FROM BD TO USER 1

In SR, the expression of ergodic rate from BD to User 1 R_c^{SR} is the same with (30). Therefore, the closed-form expression of R_c^{SR} is written as (36).

C. SLOPE ANALYSIS

In this section, we evaluate the high SNR slope, which is an important metric for ergodic rate. The slope for high SNR region is defined as

$$S = \lim_{p \to \infty} \frac{R^{(e)}(p)}{10 \log_{10} p}. \quad (38)$$

1) ERGODIC RATE FROM BS TO USER 1 IN BACKSCATTER-NOMA

From (26), it is seen that when the transmitted power goes to infinity, the ergodic rate from BS to User 1 goes to a constant based on the Appendix C. According the definition of slope in (38), we have that the slope in terms of ergodic analysis from BS to User 1 is $S_{U,1} = 0$.

2) ERGODIC RATE FROM BS TO USER 2 IN BACKSCATTER-NOMA

Similar to IV-C.1, based on (29), the ergodic rate for from BS to User 2 goes to a constant, when $p \to \infty$. According to (38), the slope in terms of ergodic rate from BS to User 2 is $S_{U,2} = 0$.

3) ERGODIC RATE FROM BD TO USER 1 IN BACKSCATTER-NOMA

To analyze the slope in terms of ergodic rate from BD to User 1, we give the following approximations. When $x \to 0$, we have $\text{Ei}(-x) \approx \ln(x) + C$ [36] and $e^x \approx 1 + x$, where C is a Euler constant. Thus, when the transmitted power p goes to infinity, the ergodic rate from BD to User 1 in (36) becomes

$$R_c^{(e)} \approx \frac{-M^2 \pi^2}{4KN\lambda_f \lambda_{v,1} \ln 2} \sum_{k=1}^{K} \sqrt{1 - \phi_k^2} \, e^{-\frac{M\phi_k + M}{2\lambda_{v,1}}} \sum_{n=1}^{N} \sqrt{1 - \varphi_n^2}$$

$$\times e^{-\frac{M\varphi_n + M}{2\lambda_f}} \left(\ln\left(\frac{4\sigma^2}{p|\beta|^2 (M\phi_k + M)(M\varphi_n + M)} \right) + C \right)$$

$$\times \left(1 + \frac{4\sigma^2}{p|\beta|^2 (M\phi_k + M)(M\varphi_n + M)} \right). \quad (39)$$

Substituting (39) into (38), we have the slope in terms of ergodic rate from BD to User 1, as follows:

$$S_c = \frac{\log_2(10)}{10} \approx 0.332. \quad (40)$$

4) ERGODIC RATE FROM BS TO USER 1 IN SR

Similar to IV-C.1, in SR, the slope in terms of ergodic rate from BS to User 1 is $S_{U1}^{SR} = 0$.

5) ERGODIC RATE FROM BD TO USER 1 IN SR

Similar to IV-C.3, in SR, the slope in terms of ergodic rate from BD to User 1 is $S_c^{SR} \approx 0.332$.

V. NUMERICAL RESULTS

In this section, numerical results are presented to evaluate the proposed performance of the backscatter-NOMA system and
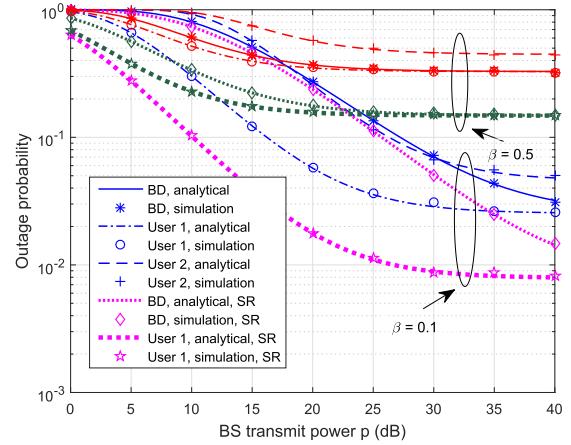

FIGURE 2. Outage probabilities versus BS transmit power *p* in backscatter-NOMA and SR.

the SR system. Here, the target rates for User 1, User 2, and BD are $R_1 = 1$, $R_2 = 1$, and $R_{c,T} = 0.1$, respectively. In addition, we set $\lambda_1 = 1$, $\lambda_2 = 0.1$, $\lambda_f = 1$, $\lambda_{v,1} = 0.8$, $\lambda_{v,2} = 0.2$, $M = 1000$, and $K = N = 8$. For the sake of simplification, we assume the noise power is 1, i.e., $\sigma^2 = 1$. Furthermore, for comparison, we also provide the performance of OMA systems, where the BS transmits $x_1(t)$, $x_2(t)$, and sine wave for User 1, User 2, and BD in three orthogonal resource blocks, respectively. In what follows, we provide the outage probability performance and the ergodic rate performance for the backscatter-NOMA system and the SR system.

A. OUTAGE PROBABILITY

Fig. 2 illustrates the outage probabilities of User 1, User 2, and BD in the backscatter-NOMA system and the outage probabilities of User 1 and BD in the SR system, with $\alpha = 0.3$. In this figure, the curves are obtained from the analytical results derived in (9), (13), (16), (17) and (18), respectively, while the dotted lines are obtained by averaging over 10^4 Monte Carlo simulations runs. From Fig. 2, it is seen that the curves of theoretical analysis perfectly match the dotted lines of the simulation results. In addition, for backscatter-NOMA system the outage probabilities of the BD and the two cellular users decrease with the increase in the BS transmit power p and converge to certain values, respectively, when p is large, which is consistent with our theoretical analysis in Section III-C. The above observation is also made in SR. The outage performance is improved with smaller β for the two cellular users in backscatter-NOMA (or User 1 in

$$R_c^{(e)} = \mathbb{E}_{f,v_1,x} \left[\log_2 \left(1 + \frac{|\beta|^2 |f|^2 |v_1|^2 |x(t)|^2}{\sigma^2} \right) \right] = \mathbb{E}_{f,v_1} \left[-\frac{1}{\ln 2} e^{\frac{\sigma^2}{p|\beta|^2 |f|^2 |v|^2}} \text{Ei} \left(-\frac{\sigma^2}{p|\beta|^2 |f|^2 |v|^2} \right) \right]$$

$$= \int_0^{+\infty} e^{-\frac{u}{\lambda_f}} \underbrace{\int_0^{+\infty} \frac{-1}{\lambda_f \lambda_{v,1} \ln 2} e^{-\frac{w}{\lambda_{v,1}} + \frac{\sigma^2}{p|\beta|^2 uw}} \text{Ei} \left(-\frac{\sigma^2}{p|\beta|^2 uw} \right) dw}_{B_6} \, du \quad (31)$$
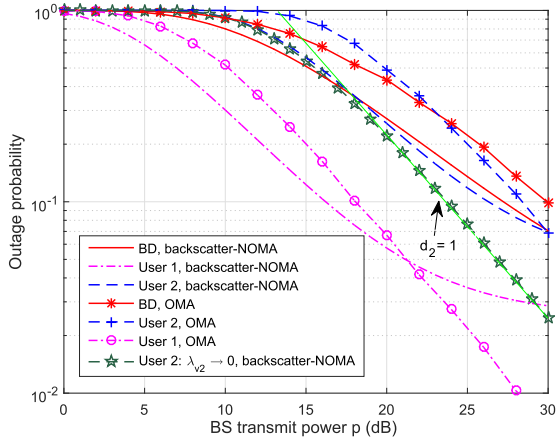
FIGURE 3. Outage probabilities for backscatter-NOMA system and OMA system versus BS transmit power *p*.

FIGURE 4. Outage probabilities for backscatter-NOMA system versus power allocation parameter α.

SR system) since the lower β means the lower backscatter link interference. For BD, the outage probability decreases as β increases at low SNR, but increases at high SNR for both backscatter-NOMA and SR systems. The reason is that if User 1 can not decode $x_2(t)$ and $x_1(t)$ successfully in backscatter-NOMA (or $x_1(t)$ in SR), the outage event happens. Furthermore, the outage probability of User 1 in SR is lower than that in backscatter-NOMA since BS serves User 1 with all power and User 1 is not required to decode $x_2(t)$ in SR. The outage performance of BD in SR is better than that in backscatter-NOMA. The main reason is that the the outage performance of User 1 is improved in SR compared with that in backscatter-NOMA.

Fig. 3 compares the outage performance for backscatter-NOMA scheme and that for OMA scheme with $\alpha = 0.3$. From this figure, it is seen that the outage performance of backscatter-NOMA is better than that of OMA when the BS transmit power p is not large enough, while is worse when p is large. The main reason is that the backscatter-NOMA system is spectrum-efficiency through exploiting the power domain, while the outage probabilities of backscatter-NOMA system have floors according to the analysis in Section III-C. This phenomenon indicates that the cellular networks can achieve the gain of the NOMA under the influence of the IoT networks when the power from BS is not large enough. In addition, we plot the curve of the outage probability of User 2 with $\lambda_{v,2} \to 0$ based on (11) in this figure. In this case, the diversity order is $d_2 = 1$, which is consistent with the analysis in Section III-C.1.

Fig. 4 plots the effect of power allocation parameter α on the outage performance with $p = 40$ dB and $\beta = 0.1$. It can be seen that the outage probability for User 2 increases with increasing α and equals 1 when $\alpha = 0.5$ due to the increase of interference and the decrease of its own message power, which validates the analysis in Section III-A.1. The outage probability of User 1 decreases first and then increases with the increase in α since User 1 needs to decode $x_2(t)$, which is consistent with the analysis in Section III-A.2.
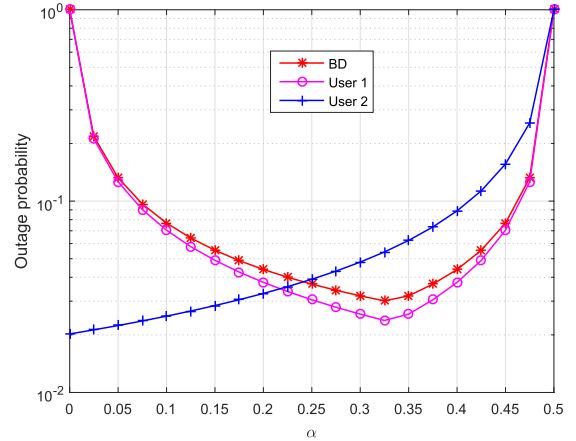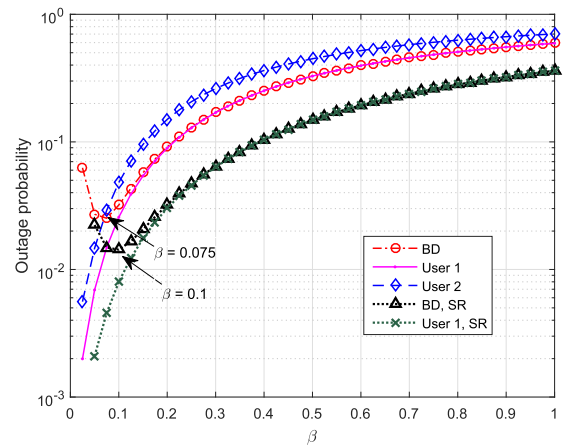

FIGURE 5. Outage performance versus reflection coefficient β in backscatter-NOMA and SR.

Fig. 5 illustrates the effect of reflection parameter β on the outage performance with $p = 40$ dB and $\alpha = 0.3$. In backscatter-NOMA, the outage probabilities $P_{out,1}$ and $P_{out,2}$ increase as β grows. The main reason is that when β increases, the interference from backscatter link increases, thereby leading to the increase in $P_{out,1}$ and $P_{out,2}$. Similar to the above observation, in SR, the outage performance of User 1 decreases with the increase of β due to the same reason. In addition, from this figure, it can be seen that the outage probability for BD decreases first and then increases with the increase in β whether for backscatter-NOMA or SR. The main reason is that when β is large, it becomes more difficult for User 1 to decode its own message successfully. However when β is small, it is easier for User 1 to decode its own message successfully, but difficult for User 1 to decode the message from BD, which is consistent with the theoretical analysis in Section III-A.3 and Section III-B.2. In addition, when $p = 40$ dB, for backscatter-NOMA, the optimal β is around 0.075, while for SR, the optimal β is around 0.1.

B. ERGODIC RATE

Fig. 6, Fig. 7, and Fig. 8 illustrate the ergodic rate from BS to User 1, the ergodic rate from BS to User 2, and the ergodic
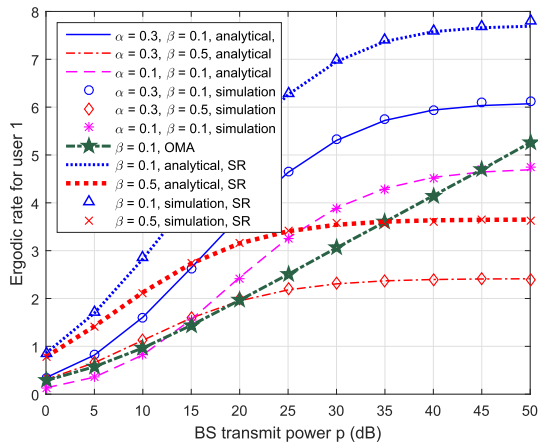
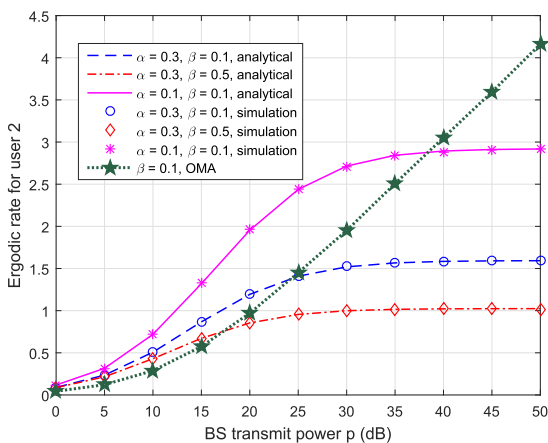**FIGURE 6.** Ergodic rate from BS to User 1 versus BS transmit power *p*.

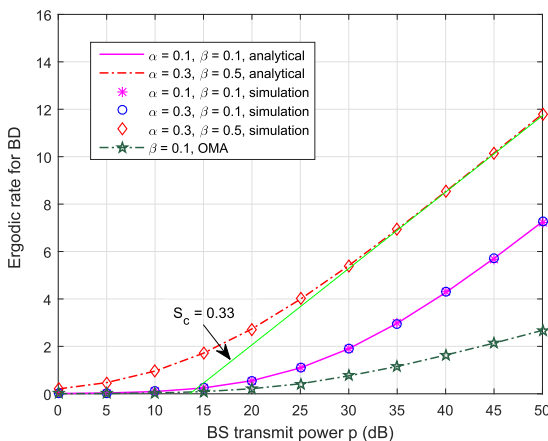**FIGURE 7.** Ergodic rate from BS to User 2 versus BS transmit power *p*.

FIGURE 8. Ergodic rate from BD to User 1 versus BS transmit power *p*.

rate from BD to User 1, respectively, versus BS transmit power *p* in the backscatter-NOMA. Fig. 6 also plots the ergodic rate from BS to User 1 versus BS transmit power *p* in the SR system. It is noteworthy that the ergodic rate from BD to User 1 in SR is the same as that in backscatter-NOMA, and thus in Fig. 8, we omit the curves in SR. Similar to Fig. 2,
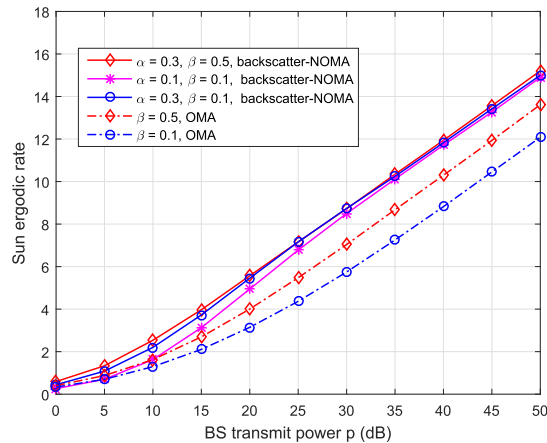

FIGURE 9. Sum ergodic rate for backscatter-NOMA system versus BS transmit power *p*.

in these figures, the dotted lines are obtained by averaging over 10^4 Monte Carlo simulations runs, while the curves are obtained from the analytical results derived in (26), (29), and (36), respectively. From Fig. 6, Fig. 7, and Fig. 8, it can be seen that the curves of analytical results perfectly match the dotted lines of the simulation results. From Fig. 6, the ergodic rate $R_{U,1}^{(e)}$ increases with the increase in α since the larger α means the higher SINR based on (4). From Fig. 7, the ergodic rate $R_{U,2}^{(e)}$ decreases with the increase in α since the SINR decreases with the increase in α according to (7). However, the ergodic rate $R_c^{(e)}$ stays unchanged as α grows. The main reason is that the BD reflects all transmit power p from the BS, not related with power allocation parameter α, which can be seen in (36). In addition, as β grows, the ergodic rates $R_{U,1}^{(e)}$, $R_{U,1}^{SR}$, and $R_{U,2}^{(e)}$ decrease due to the increase in interference from backscatter link. However, the ergodic rate $R_c^{(e)}$ increases when β increases since the SNR $\gamma_{1,c}|x$ increases with the increase in β based on (5). In these figures, we also provide the ergodic rate from BS to User 1, the ergodic rate from BS to User 2, and the ergodic rate from BD to User 1 based on OMA protocol. From Fig. 6 and Fig. 7, it is seen that the backscatter-NOMA system performs better than OMA system in terms of the ergodic rate from BS to User 1 and the ergodic rate from BS to User 2 at low SNR, while worse at high SNR. This phenomenon indicates that at low SNR, User 1 and User 2 obtain the gain of NOMA protocol in terms of ergodic rate compared with OMA system. When p is large, $R_{U,1}^{(e)}$ and $R_{U,2}^{(e)}$ are worse than ergodic rate performance in OMA protocol since the slopes of $R_{U,1}^{(e)}$ and $R_{U,2}^{(e)}$ equal to 0 according to Section IV-C.1 and Section IV-C.2 due to the existence of backscatter link interference. From Fig. 8, it is seen that the ergodic rate from BD to User 1 in backscatter-NOMA system is always better than that in OMA system. Furthermore, in Fig. 8, the slope analysis in Section IV-C.3 is verified, i.e., $S_c = 0.33$.

Fig. 9 compares the sum ergodic rate in backscatter-NOMA system and that in OMA system. From this figure, it is easy to find that the sum ergodic rate for
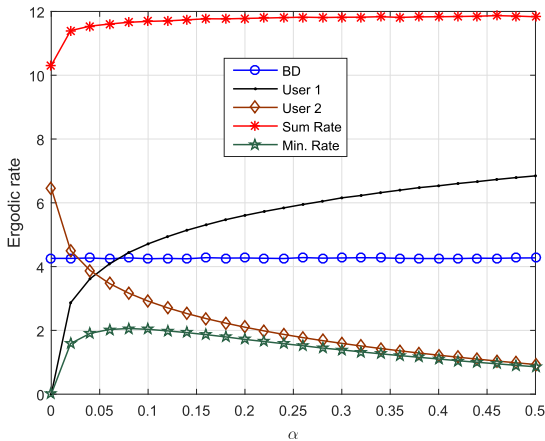
FIGURE 10. Ergodic rate for backscatter-NOMA system versus power allocation parameter α.
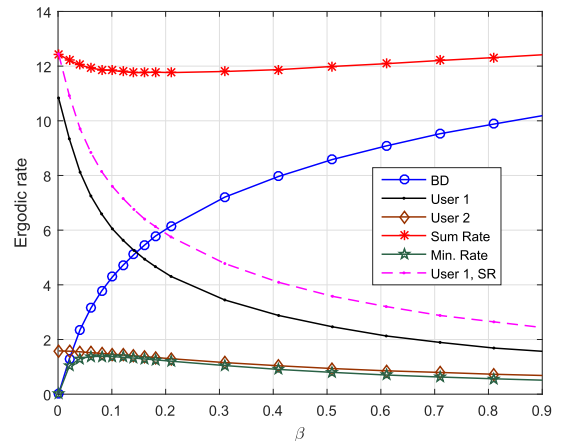

FIGURE 11. Ergodic rate versus reflection coefficient β in backscatter-NOMA and SR.

backscatter-NOMA is always better than that for OMA. This phenomenon indicates that the backscatter-NOMA system can obtain the gain of the NOMA protocol. In addition, from Fig. 9, we find the performance gap is not obvious for different α and different β.

Fig. 10 plots the effect of power allocation parameter α on the performance of ergodic rate with $p = 40$ dB and $\beta = 0.1$. Specifically, we provide the curves of the sum rate and also minimal rate, $R_{min}^{(e)} = \min\{R_{U,1}^{(e)}, R_{U,2}^{(e)}, R_c^{(e)}\}$, versus α to get the insights about the effectiveness and the fairness. In this figure, the observation about $R_{U,1}^{(e)}$, $R_{U,2}^{(e)}$, and $R_c^{(e)}$ with the increase in α is the same with that in Fig. 6, Fig. 7, and Fig. 8, which has been described. From Fig. 10, we find the sum rate increases as α grows. The main reason is that the speed of the increase in $R_{U,1}^{(e)}$ is faster than the speed of the decrease in $R_{U,2}^{(e)}$. To get more fairness, next we analyze the minimal rate between $R_{U,1}^{(e)}$, $R_{U,2}^{(e)}$, and $R_c^{(e)}$. From this figure, it is seen that the minimal rate increases first and then decreases with the increase in α. For this metric, we can obtain the optimal α to maximize the minimal rate by linear search, which is around 0.1 in the set up of this figure.

Fig. 11 illustrates the effect of reflection parameter β on the ergodic rate performance with $p = 40$ dB and $\alpha = 0.3$ in backscatter-NOMA and SR. Similar to Fig. 10, in this figure, we plot the curves of the sum rate and the minimal rate between $R_{U,1}^{(e)}$, $R_{U,2}^{(e)}$, and $R_c^{(e)}$ versus β. It is seen that the sum rate decreases first and then increases with the increase in β. When $\beta = 0$ or $\beta = 1$, the sum ergodic rate is at maximal. This behavior indicates that to maximize the sum rate, the signals from backscatter link should be zero or at maximal. In addition, the minimal rate increases first and then decreases as β grows. Thus, using this metric we can formulate an optimization problem:

$$\max_{\beta} \quad R_{min}^{(e)}. \tag{41}$$

Linear search can be used to solve the problem in (41). In the set up of this figure, when $\beta = 0.1$, the minimal rate is at

maximal, but the sum rate is at minimal. Therefore, there is a trade-off between the fairness and the effectiveness.

VI. CONCLUSIONS
This paper has studied the interrelationship of the cellular and IoT networks, and proposed a backscatter-NOMA system, which incorporates cellular NOMA and SR. We have analyzed the outage probability and the ergodic rate for the backscatter-NOMA system and the SR system. We have provided the closed-form expressions of the outage probabilities and the ergodic rate for these two systems. In addition, we have analyzed the diversity orders in terms of outage probability and the slopes in terms of ergodic rate. Numerical results have been presented to validate our analysis by comparing it with the simulation results.

APPENDIX A
If $f(x) = \frac{1}{\lambda_1} e^{\frac{-x}{\lambda_1}}$, $f(y) = \frac{1}{\lambda_2} e^{\frac{-y}{\lambda_2}}$, the PDF of $Z = X \cdot Y$ is

$$\int_0^{+\infty} \frac{1}{u} f_X\left(\frac{z}{u}\right) f_Y(u) du = \frac{1}{\lambda_1 \lambda_2} \int_0^{+\infty} \frac{1}{u} e^{\frac{-z}{\lambda_1 u} - \frac{u}{\lambda_2}} du$$

$$\overset{(a)}{=} \frac{2}{\lambda_1 \lambda_2} K_0\left(2\sqrt{\frac{z}{\lambda_1 \lambda_2}}\right),$$

where (a) can be obtained from [36].

APPENDIX B
It is reported in [36] that, for any ς and Re $\varepsilon > 0$, we have

$$\int_0^{+\infty} e^{-\varepsilon x} K_0\left(2\sqrt{\varsigma x}\right) dx$$

$$= \frac{e^{\frac{\varsigma}{2\varepsilon}}}{2\sqrt{\varepsilon \varsigma}} (\Gamma(1))^2 W_{-\frac{1}{2},0}\left(\frac{\varsigma}{\varepsilon}\right)$$

$$= \frac{e^{\frac{\varsigma}{2\varepsilon}}}{2\sqrt{\varepsilon \varsigma}} e^{-\frac{\varsigma}{2\varepsilon}} \left(\frac{\varsigma}{\varepsilon}\right)^{\frac{1}{2}} U\left(1,1,\frac{\varsigma}{\varepsilon}\right) = \frac{-e^{\frac{\varsigma}{2\varepsilon}}}{2\sqrt{\varepsilon \varsigma}} e^{-\frac{\varsigma}{2\varepsilon}} \left(\frac{\varsigma}{\varepsilon}\right)^{\frac{1}{2}} e^{\frac{\varsigma}{\varepsilon}} \text{Ei}\left(-\frac{\varsigma}{\varepsilon}\right)$$

$$= -\frac{e^{\frac{\varsigma}{\varepsilon}} \text{Ei}\left(-\frac{\varsigma}{\varepsilon}\right)}{2\varepsilon},$$

where $\Gamma(x) = (x - 1)!$ is a gamma function, $W_{k,\mu}(x) = e^{\frac{-x}{2}}x^{\mu+\frac{1}{2}}U(\mu - k + \frac{1}{2}, 1 + 2\mu; x)$ is a Whittaker function, and $U(\mu, k; z) = \frac{1}{\Gamma(\mu)}\int_0^\infty e^{-zt}t^{\mu-1}(1+t)^{k-\mu-1}dt$ is a confluent hypergeometric function with $\text{Re } \mu > 0$.

APPENDIX C
Define $f(x) \triangleq xe^x\text{Ei}(-x)$ with $x > 0$. With $E_1(x) = \int_x^{+\infty}\frac{e^{-\rho}}{\rho}d\rho$, the function $f(x)$ can also be written as $f(x) = -xe^xE_1(x)$ with $x > 0$ due to $E_1(x) = -\text{Ei}(-x)$, for positive x. For positive real value x, we have $\frac{1}{2}e^{-x}\ln(1 + \frac{2}{x}) < E_1(x) < e^{-x}\ln(1 + \frac{1}{x})$. Thus, we have $\frac{x}{2}\ln(1 + \frac{2}{x}) < xe^xE_1(x) < x\ln(1 + \frac{1}{x})$. When $x \to \infty$, we have $\lim_{x\to\infty}\frac{x}{2}\ln(1 + \frac{2}{x}) = \lim_{x\to\infty}\frac{\ln(1+\frac{2}{x})}{\frac{2}{x}} = \lim_{x\to\infty}\frac{\left(\ln(1+\frac{2}{x})\right)'}{\left(\frac{2}{x}\right)'} = \lim_{x\to\infty}\frac{1}{1+\frac{2}{x}} = 1$, Similarly, we have $\lim_{x\to\infty}x\ln(1 + \frac{1}{x}) = 1$. According to squeeze theorem, we have $\lim_{x\to\infty}xe^xE_1(x) = 1$, which means $\lim_{x\to\infty}f(x) = -1$.

APPENDIX D
PROOF OF THEOREM 2
Substituting (3) and (4) into $\Pr\{\gamma_{1,2} \geq \gamma_{2,T}, \gamma_{1,1} \geq \gamma_{1,T}\}$, we have $\Pr\{\gamma_{1,2} \geq \gamma_{2,T}, \gamma_{1,1} \geq \gamma_{1,T}\} = \Pr\{p|h_1|^2(1 - \alpha - \alpha\gamma_{2,T}) \geq \gamma_{2,T}(|\beta|^2p|f|^2|v_1|^2 + \sigma^2), \alpha p|h_1|^2 \geq \gamma_{1,T}(|\beta|^2p|f|^2|v_1|^2 + \sigma^2)\}$. It is straightforward that $\Pr\{\gamma_{1,2} \geq \gamma_{2,T}, \gamma_{1,1} \geq \gamma_{1,T}\} = 0$, when $\alpha = 0$ or $1 - \alpha - \alpha\gamma_{2,T} \leq 0$, i.e., $a \leq \alpha \leq 1$, or $\alpha = 0$. When $0 < \alpha < a$, we have $\Pr\{\gamma_{1,2} \geq \gamma_{2,T}, \gamma_{1,1} \geq \gamma_{1,T}\} = \Pr\{|h_1|^2 \geq \max\{\frac{(|\beta|^2p|f|^2|v_1|^2+\sigma^2)\gamma_{2,T}}{p(1-\alpha-\alpha\gamma_{2,T})}, \frac{(|\beta|^2p|f|^2|v_1|^2+\sigma^2)\gamma_{1,T}}{\alpha p}\}\}$. It is easy to obtain the PDFs of $|h_1|^2$, $|f|^2$, and $|v_1|^2$, which are $f_{|h_1|^2}(x) = \frac{1}{\lambda_1}e^{\frac{-x}{\lambda_1}}$, $f_{|f|^2}(u) = \frac{1}{\lambda_f}e^{\frac{-u}{\lambda_f}}$, and $f_{|v_1|^2}(w) = \frac{1}{\lambda_{v,1}}e^{\frac{-w}{\lambda_{v,1}}}$, respectively. Then, when $0 < \alpha < a$, we have

$$\Pr\{\gamma_{1,2} \geq \gamma_{2,T}, \gamma_{1,1} \geq \gamma_{1,T}\}$$
$$= \begin{cases} B_2 \triangleq \Pr\{|h_1|^2 \geq \frac{(|\beta|^2p|f|^2|v_1|^2+\sigma^2)\gamma_{2,T}}{p(1-\alpha-\alpha\gamma_{2,T})}\}, & b < \alpha \leq a; \\ B_3 \triangleq \Pr\{|h_1|^2 \geq \frac{(|\beta|^2p|f|^2|v_1|^2+\sigma^2)\gamma_{1,T}}{\alpha p}\}, & 0 < \alpha \leq b, \end{cases}$$

where $b = \frac{\gamma_{1,T}}{\gamma_{2,T}+\gamma_{1,T}+\gamma_{2,T}\gamma_{1,T}}$. It is easy to obtain $B_2 = \frac{-\lambda_1 Q_1}{\lambda_{v,1}}\text{Ei}(-\frac{\lambda_1 Q_1}{\lambda_{v,1}})e^{\frac{\lambda_1 Q_1}{\lambda_{v,1}}-\frac{Q_2}{\lambda_1}}$, and $B_3 = -\alpha Q_3$ $\text{Ei}(-\alpha Q_3)e^{\alpha Q_3 - \frac{\gamma_{1,T}\sigma^2}{p\lambda_1\alpha}}$. Thus, Theorem 2 can be proved.

APPENDIX E
PROOF OF THEOREM 3
Substituting (3), (4), and (5) into $\Pr\{\gamma_{1,2} \geq \gamma_{2,T}, \gamma_{1,1} \geq \gamma_{1,T}, \bar{\gamma}_{1,c} \geq \gamma_{c,T}\}$, we have$\Pr\{\gamma_{1,2} \geq \gamma_{2,T}, \gamma_{1,1} \geq \gamma_{1,T}, \bar{\gamma}_{1,c} \geq \gamma_{c,T}\} = \Pr\{p|h_1|^2(1 - \alpha - \alpha\gamma_{2,T}) \geq (|\beta|^2p|f|^2|v_1|^2 + \sigma^2)\gamma_{2,T}, \alpha p|h_1|^2 \geq (|\beta|^2p|f|^2|v_1|^2 + \sigma^2)\gamma_{1,T}, |\beta|^2|f|^2|v_1|^2p \geq \sigma^2\gamma_{c,T}\}$. When $a \leq \alpha \leq 1$, or $\alpha = 0$, we can get $\Pr\{\gamma_{1,2} \geq \gamma_{2,T}, \gamma_{1,1} \geq \gamma_{1,T}, \bar{\gamma}_{1,c} \geq \gamma_{c,T}\} = 0$.

Then,

$$\Pr\{\gamma_{1,2} \geq \gamma_{2,T}, \gamma_{1,1} \geq \gamma_{1,T}, \bar{\gamma}_{1,c} \geq \gamma_{c,T}\}$$
$$= \begin{cases} Q_1, & b < \alpha \leq a; \\ Q_2, & 0 < \alpha \leq b; \end{cases}$$

where $Q_1 \triangleq \Pr\{|h_1|^2 \geq \frac{(|\beta|^2p|f|^2|v_1|^2+\sigma^2)\gamma_{2,T}}{p(1-\alpha-\alpha\gamma_{2,T})}, |f|^2|v_1|^2 \geq \frac{\gamma_{c,T}\sigma^2}{p|\beta|^2}\}$ and $Q_2 \triangleq \Pr\{|f|^2|v_1|^2 \geq \frac{\gamma_{c,T}\sigma^2}{p|\beta|^2}, |h_1|^2 \geq \frac{(|\beta|^2p|f|^2|v_1|^2+\sigma^2)\gamma_{1,T}}{\alpha p}\}$. It is straightforward to obtain

$$Q_1 = \int_{\frac{\gamma_{c,T}\sigma^2}{p|\beta|^2}}^{+\infty}\int_{\frac{\gamma_{2,T}(p|\beta|^2v+\sigma^2)}{p(1-\alpha-\alpha\gamma_{2,T})}}^{+\infty}f_{|h_1|^2}(y)f_{|f|^2|v_1|^2}(v)dydv$$
$$= B_2 - B_4. \tag{42}$$

where $B_4 = \frac{2}{\lambda_f\lambda_{v1}}\int_0^{\frac{\gamma_{c,T}\sigma^2}{p|\beta|^2}}e^{-\frac{\gamma_{2,T}(|\beta|^2pv+\sigma^2)}{\lambda_1p(1-\alpha-\alpha\gamma_{2,T})}}K_0\left(2\sqrt{\frac{v}{\lambda_f\lambda_{v1}}}\right)dv$. Applying Gaussian-Chebyshev quadrature, we have,

$$B_4 \approx \frac{\pi\gamma_{c,T}\sigma^2}{K|\beta|^2p\lambda_f\lambda_{v1}}e^{-\frac{\gamma_{2,T}\sigma^2}{\lambda_1p(1-\alpha-\alpha\gamma_{2,T})}}\sum_{k=1}^K\sqrt{1 - \phi_k^2}$$
$$\times e^{-\frac{\gamma_{2,T}\gamma_{c,T}\sigma^2(\phi_k+1)}{2p\lambda_1(1-\alpha-\alpha\gamma_{2,T})}}K_0(Q_4),$$

Similarly, we can obtain $Q_2 = B_3 - B_5$, where $B_5 = \frac{2}{\lambda_f\lambda_{v1}}\int_0^{\frac{\gamma_{c,T}\sigma^2}{p|\beta|^2}}e^{-\frac{\gamma_{1,T}(|\beta|^2pv+\sigma^2)}{\lambda_1p\alpha}}K_0\left(2\sqrt{\frac{v}{\lambda_f\lambda_{v1}}}\right)dv$. Applying Gaussian-Chebyshev quadrature method, we obtain,

$$B_5 \approx \frac{\pi\gamma_{c,T}\sigma^2}{K|\beta|^2p\lambda_f\lambda_{v,1}}e^{-\frac{\gamma_{1,T}\sigma^2}{\lambda_1p\alpha}}$$
$$\sum_{k=1}^K\sqrt{1 - \phi_k^2}e^{\frac{-\gamma_{1,T}\gamma_{c,T}\sigma^2(\phi_k+1)}{2\lambda_1p\alpha}}K_0(Q_4).$$

Thus, Theorem 3 is proved.

APPENDIX F
According to the rule of integral transformation, we have

$$\int_0^{+\infty}\frac{2}{\lambda_f\lambda_{v,1}}K_0\left(2\sqrt{\frac{v}{\lambda_f\lambda_{v,1}}}\right)dv$$
$$\overset{\varrho=\sqrt{v}}{=}\frac{2}{\lambda_f\lambda_{v,1}}\int_0^{+\infty}2\varrho K_0\left(2\varrho\sqrt{\frac{1}{\lambda_f\lambda_{v,1}}}\right)d\varrho \tag{43}$$

According to [36], we have $\int_0^{+\infty}x^\mu K_v(ax)dx = 2^{\mu-1}a^{-\mu-1}\Gamma(\frac{1+\mu+v}{2})\Gamma(\frac{1+\mu-v}{2})$, based on which, (43) can be rewritten as $\frac{4}{\lambda_f\lambda_{v1}}\left(\sqrt{\frac{4}{\lambda_f\lambda_{v1}}}\right)^{-2} = 1$.

REFERENCES
[1] J. G. Andrews *et al.*, "What will 5G be?" *IEEE J. Sel. Areas Commun.*, vol. 32, no. 6, pp. 1065–1082, Jun. 2014.
[2] L. Zhang, M. Xiao, G. Wu, M. Alam, Y.-C. Liang, and S. Li, "A survey of advanced techniques for spectrum sharing in 5G networks," *IEEE Wireless Commun.*, vol. 24, no. 5, pp. 44–51, Oct. 2017.
[3] Z. Ding, X. Lei, G. K. Karagiannidis, R. Schober, J. Yuan, and V. Bhargava, "A survey on non-orthogonal multiple access for 5G networks: Research challenges and future trends," *IEEE J. Sel. Areas Commun.*, vol. 35, no. 10, pp. 2181–2195, Oct. 2017.

[4] X. You, C. Zhang, X. Tan, S. Jin, and H. Wu, "AI for 5G: research directions and paradigms," *Sci. China Inf. Sci.*, vol. 62, no. 2, p. 21301, Feb. 2019.

[5] F. Zhou, Y. Wu, Y.-C. Liang, Z. Li, Y. Wang, and K.-K. Wong, "State of the art, taxonomy, and open issues on cognitive radio networks with NOMA," *IEEE Wireless Commun.*, vol. 25, no. 2, pp. 100–108, Apr. 2018.

[6] N. C. Luong, P. Wang, D. Niyato, Y.-C. Liang, Z. Han, and F. Hou, "Applications of economic and pricing models for resource management in 5G wireless networks: A survey," *IEEE Commun. Surveys Tuts.*, to be published. doi: 10.1109/COMST.2018.2870996.

[7] M. Al-Imari, P. Xiao, M. A. Imran, and R. Tafazolli, "Uplink non-orthogonal multiple access for 5G wireless networks," in *Proc. 11th Int. Symp. Wireless Commun. Syst. (ISWCS)*, Aug. 2014, pp. 781–785.

[8] N. Zhang, J. Wang, G. Kang, and Y. Liu, "Uplink nonorthogonal multiple access in 5G systems," *IEEE Commun. Lett.*, vol. 20, no. 3, pp. 458–461, Mar. 2016.

[9] Z. Ding, Z. Yang, P. Fan, and H. V. Poor, "On the performance of non-orthogonal multiple access in 5G systems with randomly deployed users," *IEEE Signal Process. Lett.*, vol. 21, no. 12, pp. 1501–1505, Dec. 2014.

[10] Q. Sun, S. Han, C. L. I, and Z. Pan, "On the ergodic capacity of MIMO NOMA systems," *IEEE Wireless Commun. Lett.*, vol. 4, no. 4, pp. 405–408, Aug. 2015.

[11] Z. Ding, F. Adachi, and H. V. Poor, "The application of MIMO to non-orthogonal multiple access," *IEEE Trans. Wireless Commun.*, vol. 15, no. 1, pp. 537–552, Jan. 2016.

[12] Z. Ding, R. Schober, and H. V. Poor, "A general MIMO framework for NOMA downlink and uplink transmission based on signal alignment," *IEEE Trans. Wireless Commun.*, vol. 15, no. 6, pp. 4438–4454, Jun. 2016.

[13] J. N. Laneman, D. N. C. Tse, and G. W. Wornell, "Cooperative diversity in wireless networks: Efficient protocols and outage behavior," *IEEE Trans. Inf. Theory*, vol. 50, no. 12, pp. 3062–3080, Dec. 2004.

[14] Z. Ding, M. Peng, and H. V. Poor, "Cooperative non-orthogonal multiple access in 5G systems," *IEEE Commun. Lett.*, vol. 19, no. 8, pp. 1462–1465, Aug. 2015.

[15] Y. Liu, Z. Ding, M. Elkashlan, and H. V. Poor, "Cooperative non-orthogonal multiple access with simultaneous wireless information and power transfer," *IEEE J. Sel. Areas Commun.*, vol. 34, no. 4, pp. 938–953, Apr. 2016.

[16] L. Zhang, J. Liu, M. Xiao, G. Wu, Y.-C. Liang, and S. Li, "Performance analysis and optimization in downlink NOMA systems with cooperative full-duplex relaying," *IEEE J. Sel. Areas Commun.*, vol. 35, no. 10, pp. 2398–2412, Oct. 2017.

[17] V. Liu, A. Parks, V. Talla, S. Gollakota, D. Wetherall, and J. R. Smith, "Ambient backscatter: Wireless communication out of thin air," *ACM SIGCOMM*, vol. 43, no. 4, pp. 39–50, Aug. 2013.

[18] L. Zhang, Y.-C. Liang, and M. Xiao. (2018). "Spectrum sharing for Internet of Things: A survey." [Online]. Available: https://arxiv.org/abs/1810.04408

[19] Q. Zhang, P. P. Liang, Y.-D. Huang, Y. Pei, and Y.-C. Liang, "Label-assisted transmission for short packet communications: A machine learning approach," *IEEE Trans. Veh. Technol.*, vol. 67, no. 9, pp. 8846–8859, Sep. 2018.

[20] X. Kang, Y.-C. Liang, and J. Yang, "Riding on the primary: A new spectrum sharing paradigm for wireless-powered IoT devices," *IEEE Trans. Wireless Commun.*, vol. 17, no. 9, pp. 6335–6347, Sep. 2018.

[21] D. Darsena, G. Gelli, and F. Verde, "Modeling and performance analysis of wireless networks with ambient backscatter devices," *IEEE Trans. Commun.*, vol. 65, no. 4, pp. 1797–1814, Jan. 2017.

[22] G. Wang, F. Gao, R. Fan, and C. Tellambura, "Ambient backscatter communication systems: Detection and performance analysis," *IEEE Trans. Commun.*, vol. 64, no. 11, pp. 4836–4846, Nov. 2016.

[23] J. Qian, F. Gao, G. Wang, S. Jin, and H. Zhu, "Semi-coherent detection and performance analysis for ambient backscatter system," *IEEE Trans. Commun.*, vol. 65, no. 12, pp. 5266–5279, Dec. 2017.

[24] A. N. Parks, A. Liu, S. Gollakota, and J. R. Smith, "Turbocharging ambient backscatter communication," *ACM SIGCOMM*, vol. 44, no. 4, pp. 619–630, Oct. 2015.

[25] D. Bharadia, K. R. Joshi, M. Kotaru, and S. Katti, "BackFi: High through-put WiFi backscatter," *Comput. Commun. Rev.*, vol. 45, no. 4, pp. 283–296, Oct. 2015.

[26] G. Yang, Y.-C. Liang, R. Zhang, and Y. Pei, "Modulation in the air: Backscatter communication over ambient OFDM carrier," *IEEE Trans. Commun.*, vol. 66, no. 3, pp. 1219–1233, Mar. 2018.

[27] G. Yang, Q. Zhang, and Y.-C. Liang, "Cooperative ambient backscatter communications for green Internet-of-Things," *IEEE Internet Things J.*, vol. 5, no. 2, pp. 1116–1130, Apr. 2018.

[28] Q. Zhang and Y.-C. Liang, "Signal detection for ambient backscatter com-munications using unsupervised learning," in *Proc. IEEE GLOBECOM Workshop*, Singapore, Dec. 2017, pp. 1–6.

[29] H. Guo, Q. Zhang, S. Xiao, and Y.-C. Liang, "Exploiting multiple anten-nas for cognitive ambient backscatter communication," *IEEE Internet Things J.*, to be published. doi: 10.1109/JIOT.2018.2856633.

[30] Q. Zhang, H. Guo, Y.-C. Liang, and X. Yuan, "Constellation learning-based signal detection for ambient backscatter communication systems," *IEEE J. Sel. Areas Commun.*, vol. 37, no. 2, pp. 452–463, Feb. 2019.

[31] J. Guo, X. Zhou, S. Durrani, and H. Yanikomeroglu, "Design of non-orthogonal multiple access enhanced backscatter communication," *IEEE Trans. Wireless Commun.*, vol. 17, no. 10, pp. 6837–6852, Oct. 2018.

[32] D. Li and Y.-C. Liang, "Adaptive ambient backscatter communica-tion systems with MRC," *IEEE Trans. Veh. Technol.*, vol. 67, no. 12, pp. 12352–12357, Dec. 2018.

[33] D. Li, W. Peng, and Y.-C. Liang, "Hybrid ambient backscatter communi-cation systems with harvest-then-transmit protocols," *IEEE Access*, vol. 6, pp. 45288–45298, Sep. 2018.

[34] R. Long, H. Guo, G. Yang, Y.-C. Liang, and R. Zhang. (2018). "Symbiotic radio: A new communication paradigm for passive Internet-of-Things." [Online]. Available: https://arxiv.org/abs/1810.13068

[35] D. Tse and P. Viswanath, *Fundamentals of Wireless Communication*. Cambridge, U.K.: Cambridge Univ. Press, 2005.

[36] I. S. Gradshteyn and I. M. Ryzhik, *Table of Integrals, Series, and Products*. New York, NY, USA: Academic, 2014.

QIANQIAN ZHANG (S'17) received the B.S. degree in communication engineering from Jilin University, in 2016. She is currently pursuing the Ph.D. degree with the University of Electronic Science and Technology of China, China. Her research interests include transceiver design for the Internet of Things and machine learning for wireless communications.

LIN ZHANG received the bachelor's degree in communication engineering from Sichuan Uni-versity, Chengdu, China, in 2011, and the Ph.D. degree from the National Key Laboratory of Sci-ence and Technology on Communications, Uni-versity of Electronic Science and Technology of China, Chengdu, in 2017, where he currently holds a Postdoctoral position. From 2014 to 2016, he was a Visiting Student with the School of Electrical Engineering, KTH Royal Institute of Technology, Sweden. His research interests include cognitive radio, D2D communication, content caching, non-orthogonal multiple access, and short packet commu-nications. He received the IEEE GLOBECOM 2012 Best Paper Award, the Travel Grant Award, and the IEEE Region 10 Distinguished Student Paper Award, in 2016.

YING-CHANG LIANG (F'11) was a Professor with The University of Sydney, Australia, a Principal Scientist and a Technical Advisor with the Institute for Infocomm Research, Singapore, and a Visiting Scholar with Stanford University, USA. He is currently a Professor with the University of Electronic Science and Technology of China, China, where he leads the Center for Intelligent Networking and Communications and he is also the Deputy Director of the Artificial Intelligence Research Institute. His research interests include the general area of wireless networking and communications, cognitive radio, dynamic spectrum access, the Internet of Things, artificial intelligence, and machine learning techniques.

Dr. Liang was elected as a Fellow of the IEEE for contributions to cognitive radio communications. He received the Prestigious Engineering Achievement Award from the Institute of Engineers Singapore, in 2007, the Outstanding Contribution Appreciation Award from the IEEE Standards Association, in 2011, and the Recognition Award from the IEEE Communications Society Technical Committee on Cognitive Networks, in 2018. He has also received numerous paper awards, with the recent ones including the IEEE ICC Best Paper Award, in 2017, the IEEE ComSoc's TAOS Best Paper Award, in 2016, and the IEEE Jack Neubauer Memorial Award, in 2014. He was the Chair of the IEEE Communications Society Technical Committee on Cognitive Networks. He served as the TPC Chair and the Executive Co-Chair for IEEE GLOBECOM 2017. He served as a Guest/Associate Editor for the IEEE TRANSACTIONS ON WIRELESS COMMUNICATIONS, the IEEE JOURNAL OF SELECTED AREAS IN COMMUNICATIONS, the *IEEE Signal Processing Magazine*, the IEEE TRANSACTIONS ON VEHICULAR TECHNOLOGY, and the IEEE TRANSACTIONS ON SIGNAL AND INFORMATION PROCESSING OVER NETWORK. He was the Associate Editor-in-Chief of *Random Matrices: Theory and Applications* (World Scientific). He is the Founding Editor-in-Chief of the IEEE JOURNAL ON SELECTED AREAS IN COMMUNICATIONS—Cognitive Radio Series, the Key Founder and the Editor-in-Chief of the IEEE TRANSACTIONS ON COGNITIVE COMMUNICATIONS AND NETWORKING, and the Associate Editor-in-Chief of *China Communications*. He was a Distinguished Lecturer of the IEEE Communications Society and the IEEE Vehicular Technology Society. He was recognized by Thomson Reuters as a Highly Cited Researcher since 2014.

POOI-YUEN KAM (F'10) was born in Ipoh, Malaysia. He received the S.B., S.M., and Ph.D. degrees in electrical engineering from the Massachusetts Institute of Technology, Cambridge, MA, USA, in 1972, 1973, and 1976, respectively. From 1976 to 1978, he was a Member of the Technical Staff with Bell Telephone Laboratories, Holmdel, NJ, USA, where he was engaged in packet network studies. Since 1978, he has been with the Department of Electrical and Computer Engineering, National University of Singapore, where he is currently a Professor. From 1987 to 1988, he was on the sabbatical leave at the Tokyo Institute of Technology, Tokyo, Japan, under the sponsorship of the Hitachi Scholarship Foundation. He was the Deputy Dean of engineering and the Vice Dean for Academic Affairs, Faculty of Engineering, National University of Singapore, from 2000 to 2003. In 2006, he was invited to the School of Engineering Science, Simon Fraser University, Burnaby, BC, Canada, as a David Bensted Fellow. He was a Distinguished Guest Professor (Global) with the Graduate School of Science and Technology, Keio University, Tokyo, Japan, from 2015 to 2017. In 2017, he was a Visiting Professor with the Department of Electronic Engineering, Shanghai Jiao Tong University, China. Since 2018, he has been holding a visiting professorship at the University of Electronic Science and Technology of China, Chengdu, China. His research interests include the communication sciences and information theory, and their applications to wireless and optical communications.

Dr. Kam was elected as a Fellow of the IEEE for his contributions to receiver design and performance analysis for wireless communications. He is a member of Eta Kappa Nu, Tau Beta Pi, and Sigma Xi. He received the Best Paper Award from the IEEE VTC 2004-Fall, the IEEE VTC2011 Spring, the IEEE ICC 2011, and the IEEE/CIC ICCC 2015. He was a Co-Chair of the Communication Theory Symposium of the IEEE Globecom 2014. From 1996 to 2011, he served as an Editor for Modulation and Detection for Wireless Systems of the IEEE TRANSACTIONS ON COMMUNICATIONS. From 2007 to 2012, he served on the Editorial Board of PHYCOM, *Physical Communications* (Elsevier). From 2011 to 2017, he was a Senior Editor of the IEEE WIRELESS COMMUNICATIONS LETTERS.

● ● ●